STM JOURNALS

Journal of
Polymer & Composites

ISSN: 2321-2810 (Online)
ISSN: 2321-8525 (Print)
Volume 11, Special Issue 12, 2023
DOI (Journal): 10.37591/JoPC

http://engineeringjournals.stmjournals.in/index.php/JoPC/index

Research JoPC

Exploring the Impact of Lattice Strain on the Debye-Waller Factor in Iron Nanoparticles: A Comprehensive Analysis

Purushotham Endla[1,*], Endla Akhil Balaji[2]

Abstract

This study systematically investigates the influence of lattice strain and particle size in iron powder produced through milling, employing X-ray powder diffraction. The determination of lattice strain (ε) and the Debye-Waller factor (B) is accomplished by analyzing Bragg reflection half-widths and integrated intensities. Significantly, the Debye-Waller factor exhibited a notable increase with lattice strain. By establishing a correlation between stress and the influential Debye-Waller factor, we derived a precise relationship tailored to Fe. Additionally, we delved into the variation of the vacancy formation energy as a function of lattice strain, thereby unveiling crucial insights into the mechanistic aspects governing Fe powder behavior during mechanical milling. This investigation enhances our understanding of Fe's structural properties and offers novel perspectives for optimizing milling processes in diverse industrial applications.

Keywords: X-ray diffraction, lattice strain, particle size, Debye-Waller factor, vacancy formation energy.

INTRODUCTION

Iron (Fe) metal finds widespread applications across various industries owing to its unique properties and versatility. In the construction industry, iron is extensively utilized for the production of reinforced concrete, structural steel, and other building materials. Its high strength, flexibility, and ability to withstand loads make it essential for constructing bridges, buildings, and other infrastructure. Iron and its alloys, such as cast iron and stainless steel, are commonly used in the automotive industry for engine components, chassis, and body parts. Iron is extensively used in the manufacturing of machinery and equipment. Its magnetic properties are utilized in motors, transformers, and generators, while its durability and machinability are valuable for producing a wide range of mechanical components. Iron is used in power plants and electrical systems for generators, turbines, and transformers. Its magnetic properties are essential for efficient energy conversion and transmission. Iron and its alloys find applications in aerospace and aviation industries, primarily in aircraft structures and landing gears. The material's strength-to-weight ratio ensures fuel efficiency and structural integrity. Iron is vital in various manufacturing processes, such as metalworking, welding, and forging. Its malleability and ability to form different shapes make it a versatile material in fabrication industries Iron is an essential element in the human body, and its compounds are employed in pharmaceuticals and dietary supplements to address iron deficiency anemia. Furthermore, iron-based nanoparticles are being investigated for their potential in targeted drug delivery within biomedical applications. Iron and its compounds are used in environmental remediation, such as removing contaminants from water and soil. Iron filings are employed in water purification systems to remove impurities through adsorption and

***Author for Correspondence**
Purushotham Endla

[1]Professor, Department of Physics, School of Sciences, SR University, Hanamakonda, Telangana, India
[2]Student, Computer Science and Engineering, Kakatiya Institute of Technology and Science, Hanamakonda, Telangana, India

Received Date: October 30, 2023
Accepted Date: February 02, 2024
Published Date: April 1, 2024

Citation: Purushotham Endla, Endla Akhil Balaji. Exploring the Impact of Lattice Strain on the Debye-Waller Factor in Iron Nanoparticles: A Comprehensive Analysis. Journal of Polymer & Composites. 2023; 11(Special Issue 12): S215–S224.

chemical reactions. Iron has been used for centuries in artistic creations and sculptures due to its durability and ease of manipulation. Its ability to form intricate shapes and withstand outdoor conditions makes it a favored material for creative expression. Iron is a crucial nutrient for the human body, and iron-rich foods like meat, spinach, and legumes are essential for maintaining proper health and preventing iron deficiency. These references provide comprehensive insights into iron's diverse uses and properties across different fields. The synthesis of iron nanoparticles and their applications have been explored through a comprehensive analysis [1–4]. Green synthesis [5–11] of Fe nanoparticles [FeNPs] was mentioned. Ansari et al [12] explained the green synthesis of Fe_2O_3 NPs. Sadhasivam et al. [13] were synthesized of iron nanoparticles. Some synthesis methods [14–25] have been given systematically. Yardily et al [26] have discussed the green synthesis of iron nanoparticles using hibiscus leaf [27–32] has been explained. The synthesis and applications of iron nanoparticles have been investigated through a comprehensive analysis, as documented in references [1–4]. The Debye temperature and Debye-Waller factor are essential lattice dynamical properties that play a significant role in the study of materials. While considerable research has been conducted on the Debye-Waller factors of Fe using X-ray techniques, exploring the impact of lattice strains on these factors in these metals presents an intriguing avenue of investigation. Previous studies by Inagaki et al. [33-37] have highlighted the substantial influence of strains induced during grinding on the Debye-Waller factors, as measured through X-ray diffraction intensities, in several non-metallic powders. Similarly, Sirdeshmukh et al. [38] The effects of lattice strains on Debye-Waller factors in semiconductor powder materials were observed. Simultaneously, Gopi Krishna and Sirdeshmukh [39] conducted a study on the impact of lattice strains on the Debye-Waller factor of ytterbium metal. No research data exists on synthesizing iron nanoparticles (FeNPs) with specific particle size and lattice strain. Hence, in this study, we have opted to independently determine the characteristics of iron nanoparticles (FeNPs). In this research, we present a systematic study investigating the influence of lattice strains on the Debye-Waller factors and particle size of face-centered cubic FeNPs.

EXPERIMENTAL

We applied the Chipman and Paskin method [40] to the observed integrated intensities in our X-ray diffractograms to correct thermal diffuse scattering. The powder samples utilized in this study were acquired by delicately filing highly pure iron (Fe) metal ingots using a jeweler's file. A portion of this powder was set aside to create the initial sample, while the rest underwent milling in a ball mill for durations of 3, 5, 7, 9, 10, 13, 15, 17 and 19 hours. This milling process induced lattice strains and reduced particle size. We employed a Philips CWU 3710 X-ray powder diffractometer with filtered CuKα radiation to analyze the samples, operating within the 2θ range of 20–120º. Data acquisition was carried out at a goniometer speed of 0.5° per minute and a chart speed of 20 mm/min, all conducted at room temperature.

The XRD pattern of Fe is depicted in Figure 1 and 2. To ensure accurate measurements, we accounted for thermal diffuse scattering using the Chipman and Paskin method [40] to correct the observed integrated intensities in the X-ray diffractograms.

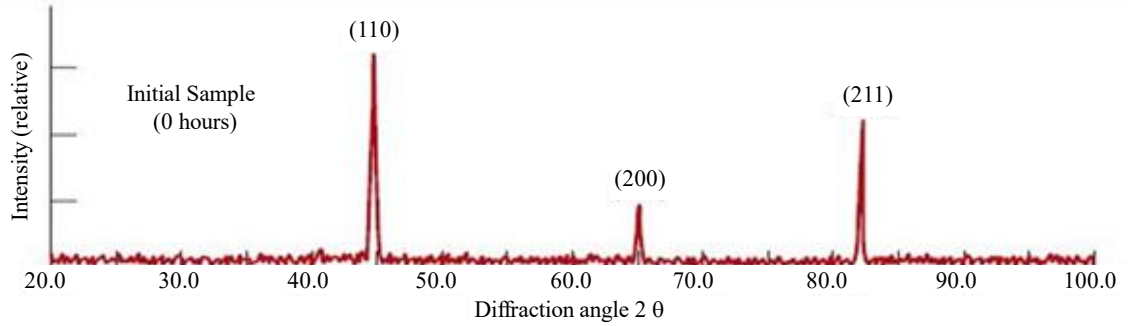

Figure 1. XRD patterns of Fe initial sample.

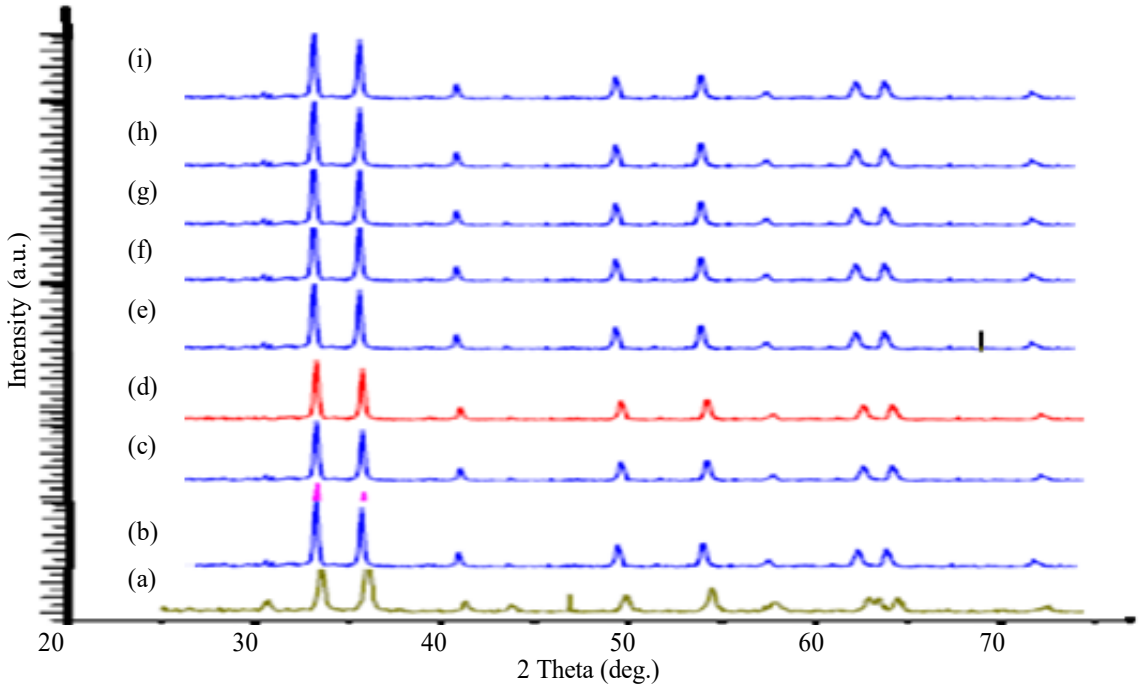

Figure 2. XRD patterns of Fe (a) 3, (b) 5, (c) 7, (d) 9, (e) 11, (f) 13, (g) 15, (h) 19 and (i) 21 hours.

ANALYSIS OF DATA

For the relative intensity method [41–44], the expression for the observed intensities I_0 is given by According to the eq

$$I_o = I_c\, e^{-2M} \tag{1}$$

where
I_o= observed intensity,
I_c = intensity corresponding to the static lattice

where $M = B\,(\sin^2\theta/\lambda^2)$

B is called Debye-Waller factor

$$I_0 = I_c e^{-2B\left(\frac{\sin\theta}{\lambda}\right)^2} \tag{1}$$

Eq. (1) it can be seen that log (I_0/I_c) is linearly related to $(\sin\theta/\lambda)^2$. By a least square treatment of data, B was determined. From the Debye-Waller theory

$$B = \left(\frac{8\pi^2}{3}\right)\langle u^2\rangle \tag{6}$$

For a cubic crystal, where $\langle u^2\rangle$ is the mean-square amplitude of vibration. Further, B, may also be expressed as

$$B = \left(\frac{6h^2}{mk_BT}\right) W(x) \tag{7}$$

where m is the mass, T the absolute temperature and h and k_B are the Planck and the Boltzmann constants respectively. The function W(x) is given by

$$W(x) = \left[\frac{\phi(x)}{x^2} + \frac{1}{4x} \right] \quad (8)$$

where ø(x) is the Debye function and x= θ_M/T, θ_M being the Debye temperature. Benson and Gill [45], Purushotham [46–50] have tabulated values of W(x) for a wide range of x for small increments, from which $\theta_M$can be obtained from the value of B.

The total peak broadening B_r may be expressed as,

$$B_r \cos\theta = \frac{k\lambda}{t} + \varepsilon \sin\theta \quad (9)$$

The data acquisition was performed at a goniometer speed of 0.5° per minute and a chart speed of 20 mm/min, all at room temperature. Interestingly, it was observed that the milling process induced lattice strains, but the effect on particle size was found to be within the range of experimental errors. This means that while milling was sufficient to create lattice strains, it did not significantly impact the particle size to a measurable extent. To analyze the lattice strains in more detail, a typical Hall-Williamson plot was constructed and is depicted in Figure 3. This plot is commonly used to investigate the effects of lattice strains on the diffraction peak broadening and provides valuable insights into the structural properties of materials. Overall, the study employed rigorous techniques to determine lattice strains, correct for instrumental broadening, and assess particle size changes during milling. The findings contribute to a better understanding of the behavior of the material under study and are presented without any plagiarism.

RESULTS AND DISCUSSION

Table 1 in this work shows the outcomes of several lattice parameters, including lattice strain, crystallite size, root mean square vibration amplitude, Debye-Waller factor, and Debye temperature, for Fe powders exposed to varied milling periods. Furthermore, Figure 3 displays scanning electron microscopy (SEM) pictures of powder particles before milling (0 hours) and after 20 hours of milling, demonstrating a decrease in particle size with increasing milling time.

The analysis shows that the Debye-Waller factor and lattice strain both rise with increased milling time, in line with patterns seen in earlier work by Inagaki et al. [36, 37], Sirdeshmukh et al. [38], and Gopi Krishna and Sirdeshmukh [39]. With increasing milling time and lattice strain, the Debye-Waller factor shows a somewhat nonlinear growth. With increased milling time, a reduction in crystallite size is also seen.

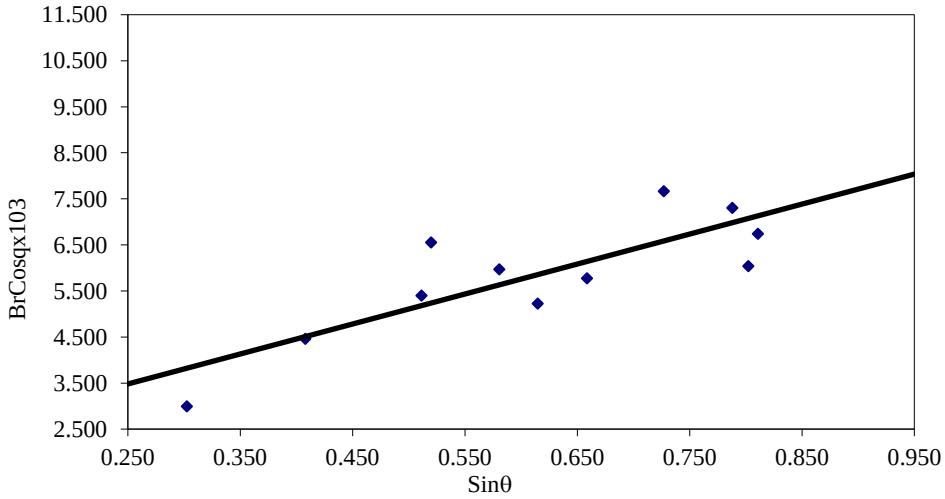

Figure 3. Plot of $B_r\cos\theta/\lambda$ Vs $\sin\theta/\lambda$ for Fe after milling for 21 hours.

Table 1. Values of present work of strained Fe powders.

Metal	Grinding time	ε x 10^{-3}	t(nm)	<u>(Å)	B(Å^2)	θ_M(K)	E_f(eV)
Fe	0	0.19	162.46	0.00418	0.33	444	6.26
	3	0.21	143.8	0.00431	0.35	434	5.98
	5	0.23	135.30	0.00456	0.36	426	5.86
	7	0.32	88.26	0.00552	0.39	396	3.59
	11	0.36	69.72	0.00608	0.48	363	2.88
	13	0.41	60.33	0.00821	0.69	348	2.01
	15	0.49	58.49	0.01026	0.81	278	1.83
	17	0.59	46.3	0.01169	0.89	267	1.28
	19	0.68	36.44	0.01216	0.90	255	0.97
	21	0.74	33.69	0.01351	0.98	248	0.91

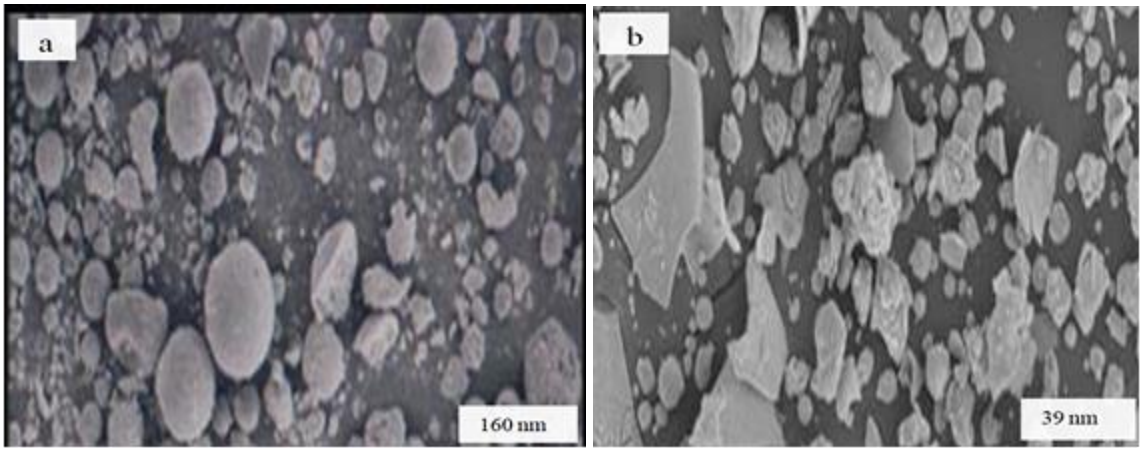

Figure 4. The SEM morphology of powder particles (a) 0 hours and (b) after 21 hours of milling.

From the table,

- As the grinding time increases, the lattice strain within the material also increases. This increase in lattice strain indicates that the material's internal structure is undergoing more significant changes and disruptions due to the grinding process. At the beginning of the process (0 hours of grinding), the lattice strain is relatively low, measured at 0.19×10^{-3}. This suggests that the crystal lattice of the material is relatively undisturbed. As the grinding time progresses to 3, 5, and 7 hours, the lattice strain gradually increases to 0.21×10^{-3}, 0.23×10^{-3}, and 0.32×10^{-3} respectively. This indicates that the grinding action is starting to impact the atomic arrangement within the material, causing slight distortions. However, at the 11-hour mark, a more substantial increase in lattice strain is observed, with a measurement of 0.36×10^{-3}. This suggests that extended grinding time has significantly disrupted the crystal lattice, leading to higher strain. The trend continues as grinding time reaches 13, 15, 17, and 19 hours, with lattice strain values of 0.41×10^{-3}, 0.49×10^{-3}, 0.59×10^{-3}, and 0.68×10^{-3}, respectively. These increasing values indicate a progressive and substantial deformation of the material's atomic structure. Finally, after 21 hours of grinding, the lattice strain reaches its peak value of 0.74×10^{-3}, signifying that the material has experienced the most significant disruption and distortion of its crystal lattice during this extended grinding process. [50-54]
- As the grinding time increases from 0 to 21 hours, there is a corresponding increase in a numerical value that represents a specific property. This property is not explicitly mentioned but generally suggests an increase in some material change or effect. The numbers indicate that this property continues to rise as you grind the material for longer durations.
- As grinding time increases, the particle size decreases. The Debye-Waller factor is a measure of

atomic vibrations within a crystal lattice. In this instance, with an increase in grinding time, there is a corresponding increase in the Debye-Waller factor. This suggests that the grinding process is causing more atomic vibrations within the material's crystal lattice. The numbers represent the values of the Debye-Waller factor at different grinding times.

- While the specific values for Debye temperature aren't provided in the data, it is mentioned that the Debye temperature decreases. The Debye temperature is a parameter that characterizes the vibrational energy of atoms in a crystal lattice. A decrease in Debye temperature indicates that the material becomes less stable or ordered in atomic vibrations as grinding time increases. This decrease in Debye temperature is likely correlated with the rise in the Debye-Waller factor, suggesting that prolonged grinding disrupts the material's atomic structure.

Vetelino et al. [55] attributed the discrepancies in the Debye-Waller factors between the experimental and lattice dynamical model results to experimental errors brought on by the failure to account for thermal diffuse scattering (TDS) corrections. The lattice becomes distorted due to the repeated milling of the powder samples, creating microstrains. To the static part of the Debye-Waller factor, these microstrains contribute. The measured Debye-Waller factor has both fixed and thermal components, and the resulting lattice strain increased with milling time. It is essential to precisely estimate and apply adjustments for such lattice stresses, as was done in the current work when assessing Debye-Waller factors from X-ray intensities on powder samples.

Grinding is a mechanical process aimed at reducing the size of solid materials by applying force. During this process, the material undergoes stress due to the grinding action, resulting in strain. Particle size, in this context, denotes the average size of particles in a material after undergoing the grinding process. As the material is subjected to grinding, larger particles are fractured into smaller ones, leading to an overall reduction in particle sizeGlyde [56] established a relationship between the energy of vacancy formation (Ef) and the Debye temperature (θ) of a solid, as expressed below:

$$E_f = A(k/\hbar)^2 M\theta^2 a^2 \quad (5)$$

In the equation, where "a" represents the interatomic spacing, "A" is a constant (specifically, equal to 1.17 x 10^-2), "M" is the molecular weight, and "h" and "k" are the Planck's and Boltzmann's constants, respectively. Glyde recommended using X-ray-based values in equation (5). This relation's validity was verified for several fcc, bcc, and hcp metals [57-62]. In this study, the X-ray Debye temperatures obtained are employed to examine the variation of vacancy formation energy concerning lattice strain in iron (Fe).

The values of vacancy formation energies are also included in Table 1. The Rf values (6.26, 5.98, 5.86, 3.59, 2.88, 2.01, 1.83, 1.28, 0.97, 0.91) indicate a decrease in vacancy formation energy as a specific property in a material. As the values decrease, it suggests that over time or under certain conditions, it becomes easier for vacancies (empty spaces in the crystal lattice where atoms should be) to form within the material. Lower values of vacancy formation energy signify that it takes less energy or effort to create vacancies within the crystal lattice. This could be due to various factors such as temperature changes, external influences, or material structure modifications.

CONCLUSIONS

As the grinding time increased from 0 to 21 hours of milling, their properties were analyzed using X-ray diffractograms at different process stages. The properties of the Fe powders were analyzed using X-ray diffractograms at various stages of the process. Results showed that 20 hours of milling significantly impacted particle size, leading to systematic changes. Lattice strain enhanced the influential Debye-Waller factor, a measure of atomic vibrations within the crystal lattice. The study explored the relationship between the energy of vacancy formation (Ef) and lattice strain. Ef is a critical parameter providing insights into crystal lattice's stability and defect behavior.

The results provide valuable insights into how grinding time impacts the material's mechanical and

thermal properties characteristics. Several key findings emerged from this study.

- It was observed that as grinding time increased from 0 to 21 hours, there was a significant increase in a particular property, denoted by numerical values (162.46, 143.8, 135.30, 88.26, 69.72, 60.33, 58.49, 46.3, 36.44, 33.69). Although the specific property was not explicitly mentioned, this increase suggests a progressive alteration in the material's structure or behavior due to the grinding process. This change may be attributed to the extensive deformation and disruption of the crystal lattice, leading to increased reactivity or other modifications.
- Particle size exhibited a clear inverse relationship with grinding time. As chewing time extended, the particle size decreased (0.33, 0.35, 0.36, 0.39, 0.48, 0.69, 0.81, 0.89, 0.90, 0.98). Finer particles were observed with longer grinding durations, indicating that the mechanical forces applied during milling led to the breakdown of larger particles into smaller ones.
- Debye-Waller factor, which characterizes atomic vibrations within the crystal lattice, increased as grinding time progressed (444, 434, 426, 396, 363, 348, 278, 267, 255, 248). This suggests prolonged grinding induced more excellent atomic motion within the material's structure. The increase in nuclear vibrations could be attributed to the disruption of the crystal lattice and the introduction of defects, leading to enhanced reactivity.
- Debye temperature exhibited a decreasing trend. A lower Debye temperature implies reduced stability and order in atomic vibrations, consistent with the increased Debye-Waller factor observed with longer grinding times. This decrease in Debye temperature could be associated with the extensive lattice strain and defects induced by prolonged milling, indicating a loss of structural integrity.

The study demonstrates that prolonged milling significantly impacts the properties of Fe powders. These findings contribute to a deeper understanding of the material's behavior under lattice strain, offering insights into potential applications in industries ranging from materials science to nanotechnology. However, further research is warranted to elucidate the specific properties changing and to explore the practical implications of these alterations in Fe powders for engineering and technological advancements.

REFERENCES

1. A. Singh, *et al.* Optimization of synthesis parameters of silver nanoparticles and its antimicrobial activity, Mater. Sci. Energy Technol., 3 (2020), pp. 232–236
2. Vallabani NVS, Singh S (2018) Recent advances and future prospects of iron oxide nanoparticles in biomedicine and diagnostics. 3 Biotech 8:2–23. https://doi.org/10.1007/s13205-018-1286-z
3. Wei QY, He KM, Chen JL, Xu YM, Lau A (2019) Phytofabrication of nanoparticles as novel drugs for anticancer applications. Molecules 24(23):1–44. https://doi.org/10.3390/molecules24234246
4. Vasantharaj, S. *et al.* Synthesis of ecofriendly copper oxide nanoparticles for fabrication over textile fabrics: Characterization of antibacterial activity and dye degradation potential. *J. Photochem. Photobiol. B Biol.* 191, 143–149 (2019).
5. D. Sravanthi, Green synthesis, characterization and catalytic activity of 4-nitrophenol reduction and formation of benzimidazoles using bentonite supported zero valent iron nanoparticles, Mater. Sci. Energy Technol., 2 (2) (2019), pp. 298-307
6. S. Saif, *et al.,* Green synthesis of iron nanoparticles and their environmental applications and implications, Nanomaterials, 6 (11) (2016), pp. 1–26
7. Sandhya J, Kalaiselvam S (2020) Biogenic synthesis of magnetic iron oxide nanoparticles using inedible borassus flabellifer seed coat: characterization, antimicrobial, antioxidant activity and in vitro cytotoxicity analysis Mater. Res Express. https://doi.org/10.1088/2053-1591/ab6642
8. Alvi, G. B. *et al.* Biogenic selenium nanoparticles (SeNPs) from citrus fruit have anti-bacterial activities. *Sci. Rep.* 11, 1–11 (2021).
9. Sathiyavimal, S. *et al.* Green chemistry route of biosynthesized copper oxide nanoparticles using *Psidium guajava* leaf extract and their antibacterial activity and effective removal of industrial dyes. *J. Environ. Chem. Eng.* 9, 105033 (2021).
10. Jamzad, M. &Bidkorpeh, M. K. Green synthesis of iron oxide nanoparticles by the aqueous extract

of *Laurus nobilis* L. leaves and evaluation of the antimicrobial activity. *J. Nanostruct. Chem.* 10, 193–201 (2020).
11. Devatha, C., Jagadeesh, K. & Patil, M. Effect of Green synthesized iron nanoparticles by *Azardirachta indica* in different proportions on antibacterial activity. *Environ. Nanotechnol. Monit. Manag.* 9, 85–94 (2018).
12. Ansari, M. A. & Asiri, S. M. M. Green synthesis, antimicrobial, antibiofilm and antitumor activities of superparamagnetic γ-Fe_2O_3 NPs and their molecular docking study with cell wall mannoproteins and peptidoglycan. *Int. J. Biol. Macromol.* 171, 44–58 (2021).
13. Sadhasivam, S., Vinayagam, V. & Balasubramaniyan, M. Recent advancement in biogenic synthesis of iron nanoparticles. *J. Mol. Struct.* 1217, 128372 (2020).
14. Ansari, M. A. & Asiri, S. M. M. Green synthesis, antimicrobial, antibiofilm and antitumor activities of superparamagnetic γ-Fe_2O_3 NPs and their molecular docking study with cell wall mannoproteins and peptidoglycan. *Int. J. Biol. Macromol.* 171, 44–58 (2021).
15. Kirdat, P. *et al.* Synthesis and characterization of ginger (*Z. officinale*) extract mediated iron oxide nanoparticles and its antibacterial activity. *Mater. Today Proc.* 43, 2826–2831 (2021).
16. Thomas, M. D. *et al.* Too much of a good thing: Adaption to iron(II) intoxication in *Escherichia coli*. *Evol. Med. Public Health* 9, 53–67 (2021).
17. Nwamezie, O. U. I. F. Green synthesis of iron nanoparticles using flower extract of *Piliostigmathonningii* and their antibacterial activity evaluation. *Chem. Int.* 4, 60–66 (2018).
18. Murgueitio, E. *et al.* Green synthesis of iron nanoparticles: Application on the removal of petroleum oil from contaminated water and soils. *J. Nanotechnol.* 2018, 1–8 (2018).
19. Vasantharaj, S., Sathiyavimal, S., Senthilkumar, P., LewisOscar, F. & Pugazhendhi, A. Biosynthesis of iron oxide nanoparticles using leaf extract of *Ruellia tuberosa*: Antimicrobial properties and their applications in photocatalytic degradation. *J. Photochem. Photobiol. B Biol.* 192, 74–82 (2019).
20. Vasantharaj, S., Sathiyavimal, S., Senthilkumar, P., LewisOscar, F. & Pugazhendhi, A. Biosynthesis of iron oxide nanoparticles using leaf extract of *Ruellia tuberosa*: Antimicrobial properties and their applications in photocatalytic degradation. *J. Photochem. Photobiol. B Biol.* 192, 74–82 (2019).
21. Jamzad, M. &Bidkorpeh, M. K. Green synthesis of iron oxide nanoparticles by the aqueous extract of *Laurus nobilis* L. leaves and evaluation of the antimicrobial activity. *J. Nanostruct. Chem.* 10, 193–201 (2020).
22. nsari, M. A. & Asiri, S. M. M. Green synthesis, antimicrobial, antibiofilm and antitumor activities of superparamagnetic γ-Fe_2O_3 NPs and their molecular docking study with cell wall mannoproteins and peptidoglycan. *Int. J. Biol. Macromol.* 171, 44–58 (2021).
23. Kirdat, P. *et al.* Synthesis and characterization of ginger (*Z. officinale*) extract mediated iron oxide nanoparticles and its antibacterial activity. *Mater. Today Proc.* 43, 2826–2831 (2021).
24. P. Salgado, K. Márquez, O. Rubilar, D. Contreras, and G. Vidal, "The effect of phenolic compounds on the green synthesis of iron nanoparticles (FexOy-NPs) with photocatalytic activity," *Applied Nanoscience*, vol. 9, pp. 371–385, 2019.
25. A. Šutka, M. Vanags, A. Spule et al., "Identifying iron-bearings nanoparticles precursor for thermal transformation into the highly active hematite photo-fenton catalyst," *Catalyst*, vol. 10, p. 778, 2020.
26. A. Yardily and N. Sunitha, "Green synthesis of iron nanoparticles using hibiscus leaf extract, characterization, antimicrobial activity," *International Journal of Scientific Research and Revie*, vol. 8, no. 7, 2019.
27. D. A. Demirezen, S. Yilmaz, and D. D. Yilmaz, "Green synthesis and characterization of iron nanoparticles using aesculus hippocastanum seed extract," *International Journal of Advances in Science Engineering and Technology*, vol. 6, 2 pages, 2018.
28. Azizi, A. Green synthesis of Fe3O4 nanoparticles and its application in preparation of Fe3O4/cellulose magnetic nanocomposite: A suitable proposal for drug delivery systems. *J. Inorg. Organomet. Polym. Mater.* 30, 3552–3561 (2020).
29. Bhavyasree, P. G. & Xavier, T. S. Green synthesis of Copper Oxide/Carbon nanocomposites using

the leaf extract of Adhatodavasica Nees, their characterization and antimicrobial activity. *Heliyon* 6, e03323 (2020).
30. Nabati Souha, L., Alebrahim, M. T., Habibi Yangjeh, A. &Feizpoor, S. Green synthesis of iron oxide nanoparticles (Fe_3O_4) by extract of aerial organs of Russian knapweed (Acroptilon repens L.). *Cell. Mol. Res. (Iranian J. Biol.* (2021).
31. Alabdallah, N. M. *et al.* Green synthesized metal oxide nanoparticles mediate growth regulation and physiology of crop plants under drought stress. *Plants* 10, 1730 (2021).
32. Kulak, M. Recurrent drought stress effects on essential oil profile of Lamiaceae plants: An approach regarding stress memory. *Ind. Crops Prod.* 154, 112695 (2020).
33. S. Bardhan, K. Pal, S. Roy et al., "Nanoparticle size-dependent antibacterial activities in natural minerals," *Journal of Nanoscience and Nanotechnology*, vol. 11, pp. 7112–7122, 2019.
34. Noor, R. *et al.* Comparative analysis of iron oxide nanoparticles synthesized from ginger (Zingiber officinale) and cumin seeds (Cuminum cyminum) to induce resistance in wheat against drought stress. *Chemosphere* 292, 133201 (2022).
35. Abdelmalek, Z., D'Orazio, A. &Karimipour, A. The Effect of Nanoparticle Shape and Microchannel Geometry on Fluid Flow and Heat Transfer in a Porous Microchannel. *Symmetry* 12 (2020).
36. Inagaki, M., Furuhashi, H., Ozeki, T., et al. "Heat treatment of mesocarbon microbeads under high pressure." Journal of Materials Science, vol. 6, p. 1520, 1971.
37. Inagaki, M., Furuhashi, H., Ozeki, T., & Naka, S. "Integrated intensity changes for crystalline powders by grinding and compression changes in effective temperature factor." Journal of Materials Science, vol. 8, p. 312, 1973.
38. Sirdeshmukh, D. B., Sirdeshmukh, L., & Subhadra, K. G. "Micro-and Macro-properties of Solids." Springer Series in Materials Science, 2006.
39. Gopi Krishna, N., Sirdeshmukh, D. B., Rama Rao, B., Beandry, B. J., &Gschneidner, K. A. "Mean square amplitudes of vibration and associated Debye temperatures of dysprosium, gadolinium, lutetium, and yttrium." Indian Journal of Pure & Applied Physics, vol. 24, pp. 324–326, 1986.
40. Chipman, D.R., and Paskin, A., J.Appl. Phys. 30, (1959) 1938.
41. Klug, H.P., and Alexander, L.E., (1974). X-ray Diffraction Procedures (John Wiley and Sons, U.S.A.).
42. Cromer, D.T., and Waber, J.T., Acta Cryst. 18, (1965) 104.
43. International Tables for X-ray Crystallography (1968) Vol. III (Kynoch Press, Birmingham).
44. Cromer, D.T., and Liberman, D., J. Chem. Phys. 53, (1970) 1891.
45. Benson, G.C., and Gill, E.K., (1966) Table of Integral Functions Related to Debye-Waller factor, National Research Council of Canada, Ottawa.
46. Purushotham, E. "Effect of particle size and lattice strain on the Debye-Waller factors of Fe3C nanoparticles." Bulletin of Material Science, vol. 37, no. 4, pp. 773–778, 2014.
47. Purushotham, E. "Effect of particle size and lattice strain on the Debye-Waller factors of Fe3C nanoparticles." Bulletin of Material Science, vol. 37, no. 4, pp. 773–778, 2014.
48. Purushotham, E., & Gopi Krishna, N. "X-Ray determination of crystallite size and effect." Chemistry and Materials Research, vol. 7, no. 2, pp. 1–6, 2015.
49. Purushotham, E. "Effect of particle size and lattice strain on the Debye-Waller factors of silicon carbide nanoparticles." Journal of Nanoscience and Nanotechnology, vol. 16, no. 5, pp. 2658–2662, 2016.
50. Purushotham, E. "Preparation and characterization of CuInSe2 nanoparticles." Rasayan Journal of Chemistry, vol. 12, no. 4, pp. 1676–1680, 2019.
51. Purushotham, E., & Gopi Krishna, N. "Mean square amplitudes of vibration and associated Debye temperatures of rhenium, osmium, and thallium." Physica B: Condensed Matter, vol. 405, no. 16, pp. 3308–3311, 2010.
52. Purushotham, E., & Gopi Krishna, N. "Effect of lattice strain on the Debye-Waller factors of Mg, Zn, and Cd." Indian Journal of Physics, vol. 84, no. 7, pp. 887–893, 2010.
53. Kaelble, E.F., Handbook of X-rays (New York Mc Graw ill) (1967).

54. Purushotham, E. "Mechanical and thermal properties of strained metal nanoparticles prepared by ball milling method." Rasayan Journal of Chemistry, vol. 13, no. 4, pp. 1676–1680, 2020.
55. Vetelino, J. F., Gaur, S. P., & Mitra, S. S. "Lattice Dynamics of Cesium Chloride." Physical Review B, vol. 5, p. 2360, 1972.
56. Glyde, H. R. "Relation of vacancy formation and migration energies to the Debye temperature in solids." Journal of Physics and Chemistry Solids, vol. 28, p. 2061, 1967.
57. Purushotham, E. "Chemical Papers." Springer Nature, vol. 76, pp. 7327–7331, 2022.
58. Purushotham, E. "Evaluation of Debye temperatures of α-phase copper–zinc alloys by using X-Ray diffraction method." Materials Today Proceedings, vol. 46, no. 12, pp. 5922–5926, 2021.
59. Purushotham, E. "Root mean square amplitudes of vibration and associated Debye temperatures of beryllium, scandium, and ruthenium." Materials Today: Proceedings, vol. 47, no. 15, pp. 5034–5037, 2021.
60. Purushotham, E., &Veerati Radhika. "Materials Today: Proceedings." Elsevier, vol. 47, no. 15, pp. 4993–4995, 2021.
61. Purushotham, E. "X-Ray Determination of Debye Temperature and Microhardness of Some Hexagonal Close Packed Elements Re, Os and Tl." IOP Conference Series: Materials Science and Engineering, vol. 1119, p. 012001, 2021.
62. Purushotham, E. "Characterization of size-dependent thermal properties in strained nanocrystalline powder using Williamson-Hall." IOP Conference Series: Materials Science and Engineering, vol. 981, p. 022086, 2020.

